



Image-based feature extraction for inline quality assurance and wear classification in high-speed blanking processes

Christian Kubik¹ · Dirk Alexander Molitor¹ · Sven Varchmin¹ · Dominik Sebastian Leininger² · Joost Ohrenberg³ · Peter Groche¹

Received: 28 July 2023 / Accepted: 4 November 2023 / Published online: 10 November 2023
© The Author(s) 2023

Abstract

Wear is one of the key factors that determine the efficiency of multi-stage processes that include blanking operations. Since wear in these processes not only causes unplanned downtime but also directly affects product quality, inline detection of wear and its effect on product quality is of major importance. However, current quality assurance (QA) methods are limited to manual offline inspection by operators at predefined intervals, so that 100% inspection of the product and description of the state of wear is not found in industrial practice. The aim of this work is therefore to develop an optical system that enables in-line acquisition of product images and the associated control of blanking-specific quality features up to stroke rates of 300 strokes per minute (spm). In order to make the system attractive to small- and medium-sized enterprises (SME), the system is designed to minimize integration and investment costs using commercially available components. By combining the system with a methodology for extracting blanking-specific features, so-called key performance parameters (KPPs), the condition of the blanked surface as a relevant quality parameter is derived directly from the workpiece image. To demonstrate the transferability of the methodology to industrial applications, two use cases are investigated. In the first case, the KPPs are used directly to determine the quality of the blanked workpiece and are compared with reference measurements. Here, the KPPs are quantified with a mean absolute error of 18 μm compared to a ground truth. In the second case, the KPPs are used to build a machine learning (ML) model to estimate the wear of the blanking tool. Here, an accuracy of 92% is achieved in classifying the actual wear state.

Keywords Blanking · Inline wear detection · Image-based quality control · Machine learning in high-speed metal forming

1 Introduction

Blanking is an essential part of many process chains in the sheet metal working industry. By combining blanking with other forming operations, multi-stage tools can be constructed that enable the manufacturing of a wide

range of products. These range from components for digitalization, such as electrical contacts or circuit boards, to consumer goods, medical components, automotive parts, and planar components such as car body panels or visible surfaces of buildings. As the blanking operation in these process chains defines the final geometric and functional product properties, reliable handling of this process step is crucial. In addition to the accuracy of the target cutting line, the characteristics of the blanked surface are a key performance parameter describing a fault-free blanking operation. According to Subramonian, the deterioration of the blanked surface is described in two ways [1]. On the one hand, the geometric properties can change, resulting in an uneven distribution of the shear zone or leading to excessive burrs. On the other hand, functional properties such as hardness distribution, sensitivity to cracking or magnetic properties can worsen. In addition, deterioration of the cutting edge can be a direct indication of a failed tool

✉ Christian Kubik
kubik@ptu.tu-darmstadt.de

¹ Institute for Production Engineering and Forming Machines, Technical University of Darmstadt, Otto-Berndt-Straße 2, 64287 Darmstadt, Germany

² Institute for Mechatronic Systems, Technical University Darmstadt, Otto-Berndt-Straße 2, 64287 Darmstadt, Germany

³ Institute of Machine Tools and Factory Management, Technical University of Berlin, Pascalstraße 8, 10587 Berlin, Germany

system (e.g., wear). Although the challenges posed by these demanding geometric and functional requirements have a major impact on process profitability, reliability, and safety, in practice, QA is limited to manual and random inspection by employees and data-based binary QA. There are four main reasons for this. (1) QA is highly employee dependent and therefore not very reproducible. (2) A detailed description of the relevant features of the blanked surface is limited. (3) When the description of blanked surface is based on data, it is binary and limited to a good/bad classification. (4) There is a long latency between the occurrence of blanked surface defects in the process and their detection in an offline QA system. Although the blanked surface is a critical factor in multi-stage processes, the authors are not aware of any industrial solution that allows 100% in-line QA of the blanked surface during blanking. With reference to industrial practice and literature, five categories are identified as barriers to an application: installation space, system dynamics, blanked surface, production rates, and cost.

Installation space: The installation space limits the integration of sensors and measuring systems in multi-stage tools. Due to the tight packing of the individual forming operations and the necessary components such as guides, blank holders, strippers, and ejectors, there is not enough space available, especially in existing tool systems. In addition, the integration of sensors must be considered in the tool design phase in order to create the necessary space and to control the properties of the tool system (e.g., rigidity of the tool system [2]). *System dynamics:* As a result of the press movement, impulse-like loads are created in the forming zone, causing the system to oscillate when the tool hits the metal strip and when the product is separated from the metal strip. On the one hand, this causes the sensor system to vibrate. On the other hand, blanked workpieces are ejected at a high speed in an uncontrolled manner due to the energy released to the system by the movement of the press. This effect is enhanced by the jamming and slugging of the blanked workpiece in the die [3]. This makes it difficult to reliably detect defined areas on the ejected product. *Blanked surface:* As the blanked surface s_d is much smaller than the cutting line s_1 , so that $s_d \ll s_1$ applies, there are high demands on the sensor system to describe the features of the blanked surface. It is known from industrial practice that multi-stage tools with a blanking operation process material with a thickness of less than 2 mm, and when processing thin sheets (e.g., stator sheets, electrical connectors), thicknesses of less than 0.5 mm are encountered. *Production rates:* With processes involving a blanking operation running at production speeds of up to 2000 spm, the real-time capability of the measurement system is particularly important. This means that data acquisition, processing, and the return of blanked surface information must take place within a single stroke [4]. *Cost:* In addition to the technical challenges, the

economic viability of the system must also be taken into account. For SMEs in particular, the investment required for such a sensor system, including software and hardware, must be kept as low as possible to achieve a direct return on investment in the shortest possible time.

Therefore, the aim of this work is to develop an optical system that allows the direct detection of the blanked surface as a critical parameter in a multi-stage process with a high degree of precision. Thereby, the quantification of the properties of the blanked surface is not limited to the base area (from small plug-in contacts to large automotive outer skin parts) of the workpieces, but mainly to the thickness of the components. The authors focus on an optical system as it allows a direct, qualitative, and quantitative inspection of the blanked surface. Indirect, data-based model estimation using time series as input (e.g., force or acceleration) should not be considered, as such supervised approaches require large amounts of labeled data. In particular, the generation of labeled data for fault conditions is costly and time-consuming for the company due to the low probability of occurrence and high technical effort. In this way, the system can generate information about the current state of the product and assign it as a label to the sensorial acquired process data for the further training step of a machine-learning model. The goal of the optical system in the context of modeling is therefore the inline preparation of labels for the training process.

In addition, a methodology will be developed to automatically evaluate images of the blanked surface and to enable segmentation and extraction of the relevant features. In the design of the optical system and the underlying methodology, particular attention will be paid to the use of commercially available components (software and hardware) to keep the investment requirements low. To demonstrate the functionality of the system, two use cases are investigated. In the first case, the quality features of the blanked surface, the so-called key performance parameters (KPP), are derived from the acquired images. Their ability to quantify the blanked surface is compared and evaluated with the time-consuming microscope inspection used in industry. In the second case, since there is a direct correlation between the wear condition of the blanking tool and the product properties, a classification model to describe the wear state of the tool is derived from the KPPs. It is expected that high performance of the model will be achieved by extracting high-quality features of the blanked surface.

In order to achieve these results, the paper is structured as follows: Section 2 gives an overview of existing methods in optical QA of forming processes and the application of existing systems and their limitations. The potential of image-based monitoring compared to indirect methods is also discussed. In Section 3, the experimental setup is shown and a correlation between tool wear and blanked surface degradation from preliminary investigations is demonstrated. The methodology for evaluating and extracting the KPPs is then

presented. Section 4 describes the extracted KPPs and their suitability for quantifying the quality of blanked surface. In Section 5, an SVM for classifying wear states based on the extracted KPP is presented. Finally, Section 6 summarizes the results and provides a roadmap for future work.

2 Optically based quality assurance during forming

Monitoring of forming processes, especially sheet metal forming processes, has been part of the literature for several decades. Thereby, the monitoring is mainly based on the use of time series, as there is a known way to generate the necessary database. The most common monitoring systems are based on empirical rules such as threshold [5, 6], windows or envelopes [7], and linear discriminant functions [8] using force [9], temperature [10], or acceleration [11] as input signals. As the amount of data available in production increases, more detailed estimates of faulty process states using ML applications have become part of current research [12]. One of the first studies in this area was presented by Koh, who used a Haar transformation to extract features from a strain gauge–based force signal with threshold detection to describe discrete fault types [13]. In his work, Ge et al. presented a support vector machine (SVM) with different kernel functions to classify faulty process states during blanking, using strain gauge–based force signals as input to this classifying ML model. The authors' result demonstrated the potential of ML by achieving a successful fault detection rate of up to 99% [14]. Beyond these simple fault detection use cases, increasingly complex problems are being solved through the application of ML. For example, Hambli et al. presented a backpropagation neural network for predicting burr height formation on blanked workpieces, taking into account tool clearance and wear condition [15]. In addition, Kubik et al. demonstrated that an SVM combined with features from a force signal extracted with a principal component analysis (PCA) was able to classify six wear states during blanking with 100% accuracy [16]. With the trend towards describing increasingly complex process relationships, deep learning (DL) models are being applied to the underlying problems. For example, Huang and Dzulfikri demonstrated that a convolutional neural network (CNN) was able to discriminate between seven wear states with over 99% accuracy [17]. The authors transformed acceleration signals into the frequency domain and used the power density spectrum as input to a one-dimensional CNN. Unterberg et al. captured magnetic Barkhausen noise from multiple coils and used it to generate recursion plots that served as input to a one-dimensional CNN [18]. Using this model, they were able to classify whether a section of material belonged to the beginning, middle, or end of a coil.

As the literature shows, these monitoring approaches in sheet metal forming processes are mainly based on time series, although images could directly represent critical quality features of the product. In production, a distinction is made between in-line and off-line optical quantification of these features. While offline systems often involve the use of handheld devices, mobile measuring stations, or collaborative robots, inline optical measurement is mainly carried out by sensors mounted on machines or robots [19]. The images are captured using lasers, projections (e.g., fringe projection), interferometry, or (high-speed) cameras.

Currently, optical systems are mainly used for geometric and dimensional inspection or surface detection. In this context, Tran and Ha proposed a high-resolution camera and multi-line laser to measure the gap and geometric dimensions of car body parts during the assembly process. The system allowed complex surfaces to be measured directly inline on the vehicle [20]. Mannan et al. extracted features from images, combined them with sound data, and fed the data into a neural network to describe different geometric states of a milling tool [21]. To validate the actual geometric shape of the tool, the results were validated with ground truth from an optical microscope. Chen et al. captured images of a milling tool and extracted the contour using a Sobel operator. By applying subpixel routine, the tool contour was determined with an accuracy of $\pm 2 \mu\text{m}$ [22]. Gupta and Ramen determined surface roughness during turning by analyzing images of a laser scattering pattern at rotation speeds ranging from 140 to 285 revolutions per minute (rpm) [23]. By extracting the gray levels in a histogram, the surface roughness heights were determined independent of the ambient lighting. Lee et al. proposed digital image processing to automatically detect cracks in aluminum alloys [24]. The images were captured with a microscope and converted into binary images. With this procedure, cracks with a width of $0.5 \mu\text{m}$ or larger were detected and segmented. Myant et al. demonstrated an optical interferometer to measure the lubricant film thickness during a sliding motion on an elastic surface [25]. The lubricant film thickness is measured continuously as KPP in the range of 50 to $400 \mu\text{m}$.

Since there are a large number of scientific papers in the literature using optical systems for geometric and dimensional inspection or surface detection, the authors refer to surveys from Catalucci et al., Mohan and Poobal, and Qi et al. which provide a good overview of existing methods and approaches in this field [19, 26, 27].

Although the literature shows that optical systems offer a great potential for inline QA, especially in production environments, their transfer to blanking processes is limited. To the authors' knowledge, there are only two papers in the literature that address optical image analysis for QA during blanking. In this context, Molitor et al. proposed a CNN to classify 16 wear states during blanking. The authors acquired offline 7440 images of the parts to train the network

to classify the wear state with 99% accuracy [28]. Since there is no direct extraction of KPP to determine the product quality of the blanked workpiece, and the image acquisition is done offline, the presented work is not suitable for inline QA of the blanked surface. Another promising approach for the direct, inline quantification of the quality of blanked workpieces in the form of the blanked surface is presented by Lorenz et al. [29]. The authors developed a system consisting of a camera with a CMOS sensor and a laser as a light source to measure the blanked surface on a sheet metal strip. However, the work is limited to the detection of the blanked surface on the sheet metal strip, so that a detection of the quality of the blanked workpieces is not possible. In addition, the hardware of the optical system takes up a lot of space, and the combination of camera and laser results in high calibration effort and cost.

In summary, the detection of quality features of blanked workpieces, especially the blanked surface, is not considered in the literature. Although the KPPs of the blanked surface is crucial for the selection between a good product and a scrap product, there are no methods and applications that allow an inline determination even at high production rates. In Section 1, the authors show that the four challenges *installation space*, *blanked surface*, *system dynamics*, and *cost* are the main reasons for the lack of implementation in the industrial environment.

3 Materials and methods

In this section, the experimental setup of the blanking process and image data acquisition is described. In addition, the methodology considering the steps of preprocessing and transformation to extract the KPP is explained in detail. According to Kubik et al., the methodology proposed in this study is related to the Knowledge Discovery in Time series and Image data for Engineering Application (KDT-EA) process model [30]. This provides a systematic approach for knowledge discovery in process data (image data or time series) based on the phases of data acquisition, preparation, transformation, and modeling as well as a final validation step. Since the KPPs are used to classify wear in Section 5, the influence of a worn tool train on the blanked surface is investigated.

3.1 Blanking process

The blanking process is characterized by a vertical movement during which the tool penetrates the die and defines the final geometrical and functional characteristics of the workpiece [31]. During the operation, the workpiece is separated from the sheet metal strip without removing any material. According to Hohmann et al., the blanking process is divided into three phases [32]. During the punch phase (I), the tool

hits the sheet and begins to deform elastically. As the tool continues to penetrate, the material is plastically deformed until the maximum shear stress is reached. At this point, the material breaks, as indicated by an abrupt drop in process force. In the following push phase (II), the tool pushes the workpiece out of the die and reaches its bottom dead center. In the withdraw phase (III), the backstroke movement of the ram pulls the tool out of the material, and the sign of the process force reverses due to clamping effects.

In addition to the three phases, the process is characterized by the properties of the blanked workpiece. According to Lange, these properties are quantified by form, dimensional, and positional errors. While dimensional and positional errors are caused by geometric deviations of the tool or an offset between the punch and die, form errors occur during the plastic deformation of the workpiece. In this context, form errors describe the quality features of the blanked surface as a function of tool (clearance, wear, cutting line, etc.), semi-finished product (sheet thickness, tensile strength, alloy composition, etc.), or process parameters (temperature, lubrication, stroke speed). According to the German Institute for Standardization (DIN EN 10140), these form errors are divided into the rollover zone h_e , the shear zone h_1 , the rupture zone h_f , and the burr height h_b [33]. During the last decades, many experimental and empirical studies have been carried out to investigate the main parameters of the blanking process that influence the evaluation of these form errors. In particular, it has been shown that a change in the tool contour has a significant effect on the formation of the blanked surface [34, 35]. For example, Hernández et al. demonstrated that increasing abrasive wear leads to a modification of the blanked surface of blanked workpieces [36, 37]. They found that a higher wear volume leads to burr formation and an increase in the rollover zone. A similar correlation was found by Hambli, who showed a strong dependence of the cutting edge radii on the burr formation in experimental investigations [15]. However, since the literature only examines the influence of wear on individual features of the blanked surface and the maximum cutting edge radii investigated are limited to 0.2 mm, the dependence of all blanked surface KPPs (h_e , h_1 , h_f , and h_b) on the cutting edge radii up to 0.50 mm was determined in preliminary tests [37]. Kubik et al. demonstrated that the morphology of the blanked surface changes as a function of several parameters. Clearance, cutting edge radii, and tensile strength of the semi-finished product were identified as the main influencing factors. Other parameters, such as the temperature profile, the tribological system, the dynamic behavior of the die and press, or the varying properties of the semi-finished product, always have an indirect but small influence on one or more of the main factors.

The preliminary work has shown that the burr on the part increases significantly with increasing cutting edge radii. On the other hand, if the rollover zone remains constant

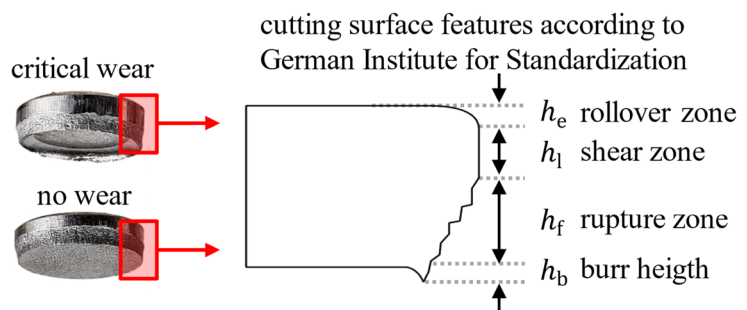
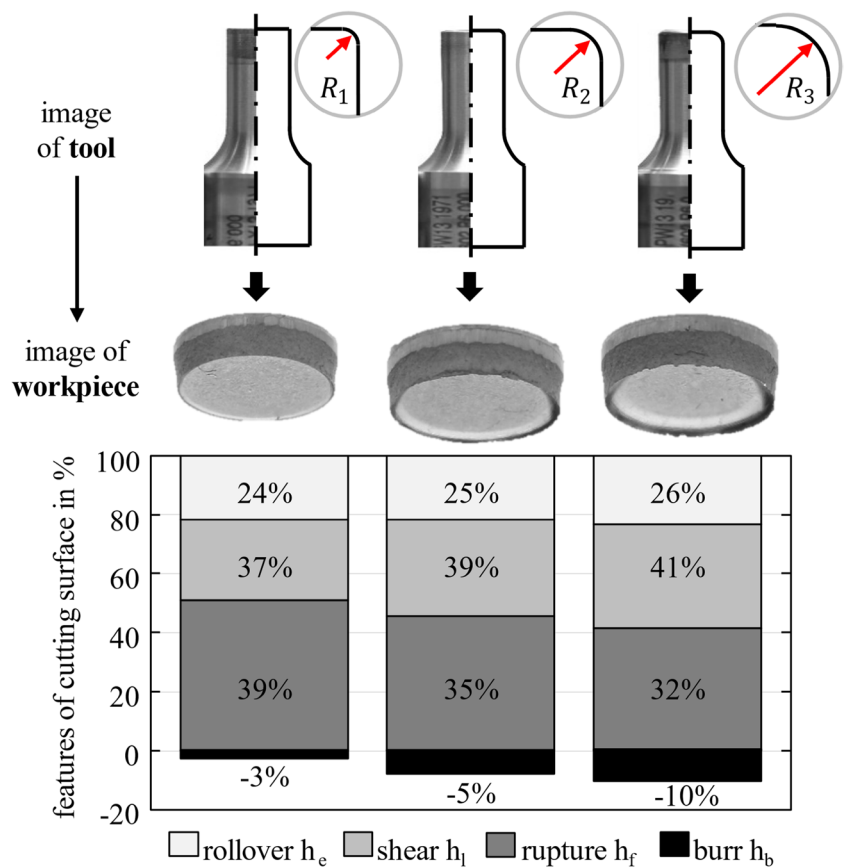
and the percentage of the shear zone increases slightly, the percentage of the fracture zone will increase. As the clearance is reduced, the shear zone increases significantly while the rollover and fracture zones decrease. A similar trend is seen in the reduction of tensile strength. Here, the rollover zone decreases, but the fracture zone increases due to the high material hardness and associated brittleness, resulting in a low shear zone fraction. The main influencing factors identified are always the result of a change in the system of tool, material, and press. For example, wear not only results in a rounding of the cutting edge radii, but also in a change in the clearance due to adhesions or breakouts on the lateral surface. Similarly, dynamic effects such as increased stroke rates or insufficient rigidity of the press or tooling system

can cause misalignment between the punch and die, which affects the clearance. Other parameters, such as temperature profile, lubrication, or tool material properties, have little or no effect on cutting edge development and can therefore be neglected. Figure 1 shows the appearance of the blanked surface for one of the three main influence factors, the cutting edge radii, for three abrasive wear states ($R_1=0.1$ mm, $R_2=0.3$ mm and $R_3=0.5$ mm).

3.2 Experimental setup

All experiments were conducted on a Bruderer high speed mechanical press (BSTA 810). The press parameters were set to a stroke distance of 51 mm and a stroke speed of 200

Fig. 1 Dependency of blanked surface feature on abrasive wear state, characterized by rounded cutting edge of the blanking tool



spm. The tool consisted of a 6-mm-diameter cylindrical punch and a 6.3-mm internal diameter die, resulting in a clearance of 0.15 mm. A cold-rolled 1.0347 steel with a thickness of 2 ± 0.05 mm, a tensile strength of 299 ± 2.90 MPa, and an elongation of break of $33.6 \pm 1.22\%$ was used. The blanking tool consists of a lower and an upper part, which are connected to each other by four columns. The cylindrical punch is connected to the adapter plate in the upper tool via a plunger. In conjunction with the movement of the ram, the punch penetrates the sheet metal (punch phase), and the workpiece is pushed out of the die (push phase). The workpieces then fall onto a collection chute, which transports them to a motorized wheel with pockets. A conveyor picks up the workpieces stroke by stroke and rotates them forward. At the top of the conveyor, two camera systems (camera, Basler AG—acA1600-60gm and lens, K.K. Ricoh—FL-CC2514A-2M) capture the image data orthogonal and at an angle of 45° to the blanked surface of the workpiece. Since the conveyor is moved in discrete steps, the images are taken during the short standstill period. At a stroke rate of 300 spm, considering the time for acceleration and deceleration of the conveyor, a standstill time of 0.05 s is obtained. Figure 2 shows the blanking tool and the optical system, which consists of cameras, lenses, a collection chute, and a conveyor. In addition to the ability to retrofit the optical system to capture workpiece images without high integration effort or capital cost, the use of commercially

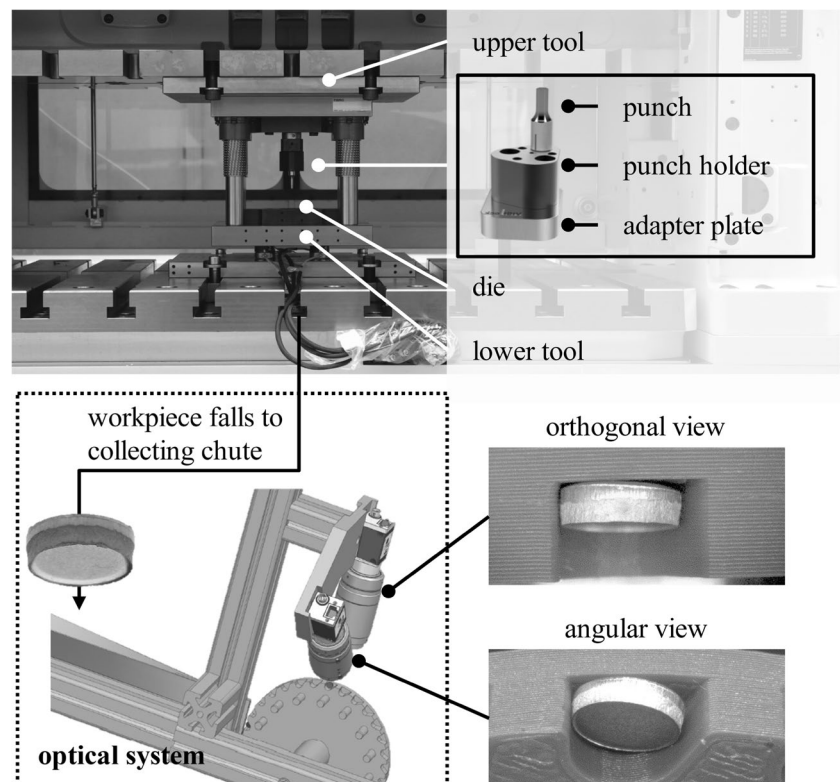
available components reduces the total cost of the optical system to less than \$800.

It should be noted at this point that it is not possible to capture the cutting line over the entire circumference with the camera system shown. In the case of a cylindrical workpiece, a range of approximately 160° can be analyzed after subtracting the distortion around the center axis of the workpiece. Inhomogeneities of the cutting line due to local defects of the punch or die, as well as variations in the material properties, can therefore only be detected to a limited extent. This applies in particular to the examination of rotationally symmetrical workpieces that have more complex cutting lines (e.g., concave or convex) or undercuts. In this case, before the optical system is designed, it must be determined based on process knowledge where critical areas of the cutting line lie that must be monitored from the perspective of quality assurance. To obtain an overall view of the distribution of the cutting lines over the circumference of the component, it may be necessary to add further cameras with different viewing angles.

3.3 Image acquisition

In order to prove the suitability of the method to be developed for the extraction of KPPs from the blanked surface, images are acquired with the optical system shown in Fig. 2. The images (orthogonal and angular view) with a size of

Fig. 2 Tool assembly for performing the blanking operation and the downstream optical system for capturing workpieces images at 300 spm in orthogonal and angular views


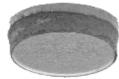

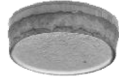












1602 × 1202 pixels are transmitted through the ethernet communication protocol GigE Vision to a microcontroller (National Instruments CompactRIO 9047). Since a realistic wear development is to be simulated and its influence on the blanked surface is to be represented via the KPPs, seven artificial wear states of the cutting edge radii up to 0.6 mm are generated. By generating seven different wear states, with an average of 3781 blanked parts per state, a realistic wear development that would require more than 300,000 strokes is mapped to a total of 26,473 strokes. This results in a data set of angular images $X_{ang} \in \mathbb{R}^{m \times n \times k}$ (45° angle to the blanked surface) and orthogonal images $X_{orth} \in \mathbb{R}^{m \times n \times k}$ (orthogonal to blanked surface) and corresponding labels $r \in \mathbb{R}^{1 \times k}$, where m and n are the image size and k is the number of observations (captured image) per wear state. Table 1 summarizes the underlying labeled data set. At this point, the authors note that a critical wear condition is not uniformly defined, and literature suggests a value between 0.20 mm and 0.40 mm, depending on the material, tooling system, and quality requirements [38, 39]. Since the evaluation of a critical wear state must be determined individually by the company and depends on the tolerable deviations of the workpiece from the target specifications, a greater value of 0.60 mm is determined in this work. This ensures that the developed method covers a wide range of possible deviations and is therefore applicable in practice for most blanking process operators.

Table 1 Overview of the labeled dataset consisting of angle and orthogonal images of blanked workpieces and the wear state represented by the cutting edge radii

3.4 Image preprocessing

Based on the image acquisition, each wear state provides k_i image pairs with a size of 1602 × 1202 pixels, depending on the wear state (see Table 1). To keep the amount of data to be processed as small as possible for the subsequent preprocessing and transformation steps, the region of interest is cropped in a first operation. This reduces the image area to be analyzed, resulting in $X_{i,ang} \in \mathbb{R}^{404 \times 899 \times k_i}$ and $X_{i,orth} \in \mathbb{R}^{600 \times 900 \times k_i}$. Filtering and contrast adjustments are neglected in this study because they distort the information value of the images and do not improve the performance of the ML model. While in the first step, a preprocessing is performed to remove images that are not suitable for further evaluation, in the second step, the KPPs are extracted by transforming and parameterizing the images. During the preprocessing, in order to quantify the insufficient images that are misplaced in the conveyor pocket, a normalized correlation coefficient between a reference image t and a workpiece image f is determined [40]. In Eq. (1), $f(x, y)$ denotes the intensity value of the image with size $M_x \times M_y$ at the point (x, y) $x \in \{0, \dots, M_x - 1\}$, $y \in \{0, \dots, M_y - 1\}$ and t the pattern of the reference image with size $N_x \times N_y$. The normalized cross correlation γ is then calculated at each point (u, v) for f and the reference image t .

| label r_i edge radii | image data $X_{i,orth}$ & $X_{i,ang}$ | workpiece image |
|---|---|---|
| $r_1 = 0$ mm  | $X_{1,orth} \in \mathbb{R}^{1602 \times 1200 \times 3360}$ $X_{1,ang} \in \mathbb{R}^{1602 \times 1200 \times 3360}$ |  |
| $r_2 = 0.1$ mm  | $X_{2,orth} \in \mathbb{R}^{1602 \times 1200 \times 3463}$ $X_{2,ang} \in \mathbb{R}^{1602 \times 1200 \times 3463}$ |  |
| $r_3 = 0.2$ mm  | $X_{3,orth} \in \mathbb{R}^{1602 \times 1200 \times 3364}$ $X_{3,ang} \in \mathbb{R}^{1602 \times 1200 \times 3364}$ |  |
| $r_4 = 0.3$ mm  | $X_{4,orth} \in \mathbb{R}^{1602 \times 1200 \times 3873}$ $X_{4,ang} \in \mathbb{R}^{1602 \times 1200 \times 3873}$ |  |
| $r_5 = 0.4$ mm  | $X_{5,orth} \in \mathbb{R}^{1602 \times 1200 \times 4062}$ $X_{5,ang} \in \mathbb{R}^{1602 \times 1200 \times 4062}$ |  |
| $r_6 = 0.5$ mm  | $X_{6,orth} \in \mathbb{R}^{1602 \times 1200 \times 4079}$ $X_{6,ang} \in \mathbb{R}^{1602 \times 1200 \times 4079}$ |  |
| $r_7 = 0.6$ mm  | $X_{7,orth} \in \mathbb{R}^{1602 \times 1200 \times 4172}$ $X_{7,ang} \in \mathbb{R}^{1602 \times 1200 \times 4172}$ |  |

$$\gamma(u, v) = \frac{\sum_{x,y} (f(x, y) - \bar{f}_{u,v}) (t(x - u, y - v) - \bar{t})}{\sqrt{\sum_{x,y} (f(x, y) - \bar{f}_{u,v})^2 \sum_{x,y} (t(x - u, y - v) - \bar{t})^2}} \tag{1}$$

$$\bar{f}_{u,v} = \frac{1}{N_x N_y} \sum_{x=u}^{u+N_x-1} \sum_{y=v}^{v+N_y-1} f(x, y) \tag{2}$$

In Eq. (2), $\bar{f}_{u,v}$ denotes the mean value of $f(x, y)$ within the area of the reference image t shifted to (u, v) , and \bar{t} is the mean value of the reference image. The maximum value of γ shifted to (u, v) in orthogonal direction ($\gamma_{\max, \text{orth}}$) and in angular direction ($\gamma_{\max, \text{ang}}$) indicates how accurately a current image of the workpiece matches the reference. A strong match between the pattern of the reference and the current image is quantified by a high normalized correlation coefficient. By setting a critical value, misplaced, excessively tilted or missing workpieces in the conveyor pockets can be identified and sorted out. Figure 3a shows the categories of misplaced or missing images in the angle and orthogonal views, as well as the image

representation of a reference workpiece t . In the angular direction, an additional distinction is made between the interference of the maximal normalized correlation coefficients right way up (RWU) $\gamma_{\max, \text{ang}_{\text{RWU}}}$ and the maximal normalized correlation coefficients upside down (USD) way up $\gamma_{\max, \text{ang}_{\text{USD}}}$.

Figure 3b shows the distribution of the maximum normalized correlation coefficient for each of the seven wear states, where each point represents a part image. To remove the erroneous images, an empirical limit is defined by the following inequalities (3) and (4), which must be satisfied for the angular and orthogonal views.

angular view

$$\gamma_{\max, \text{ang}_{\text{RWU}}} > 0.65 \text{ and } \gamma_{\max, \text{ang}_{\text{RWU}}} < \frac{5}{16} + \frac{5}{8} \cdot \gamma_{\max, \text{ang}_{\text{USD}}} \tag{3}$$

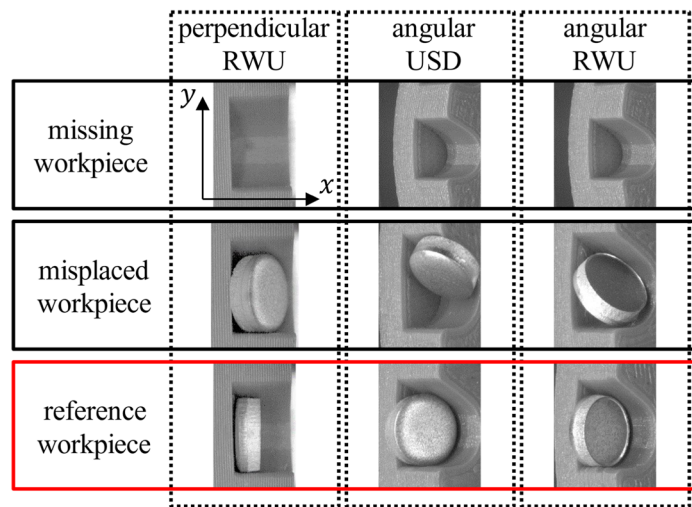
perpendicular view

$$\gamma_{\max, \text{orth}_{\text{RWU}}} > 0.75 \tag{4}$$

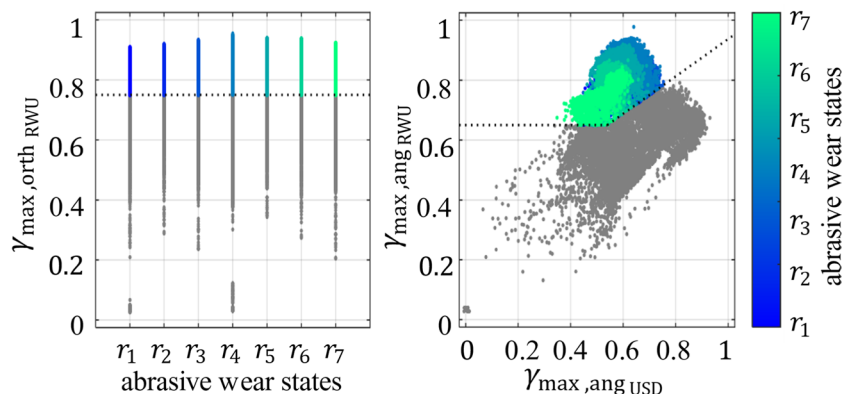
The empirical bounds given to the inequalities depend on the process configuration and must be individually defined

Fig. 3 Rejection of misplaced workpieces depending on the maximum normalized correlation coefficient γ_{\max}

a) misplaced and missing workpieces compared to a reference image



b) maximum correlation coefficient clustered in seven wear states



for transfer to similar configurations. When selecting the bounds, care must be taken to set them conservatively (false negative classification) so that all detected false workpiece images are eliminated. Table 2 shows that, especially at high states of wear, almost 80% of the captured images are rejected, which is due to the strong irregularity in the burr area and the excessive rollover zone. On average, however, nearly 30% of the workpiece images are captured correctly, resulting in an analyzable image pair. In other words, every third workpiece is subjected to QA, which results in a QA interval of 0.6 s at a stroke speed of 300 spm.

3.5 Image transformation

According to the KDT-EA process model, data preprocessing is followed by a transformation of the image data, in which relevant quality features of the blanked surface (KPP) are extracted from the workpiece images. The transformation identifies distinctive lines on the blanked surface from which the KPP are extracted. The transformation consists of three steps: segmentation, contour finding, and parameterization.

Segmentation: During the segmentation step, the workpiece image is divided into different regions using the Random Walker algorithm. According to Fig. 1, the blanked surface for the orthogonal view is segmented in two regions (area I – h_e and h_1 ; area II – h_f and h_b), while the angular view is segmented in three areas (area I – h_e and h_1 ; area II

– h_f ; area III – slug underside). To apply the Random Walker algorithm, the areas to be segmented must be approximately predefined by geometric masks as shown in Fig. 4b. According to Wechsler and Kidode, the algorithm assigns undefined pixels to the predefined masks according to the highest probability by concatenating random movements [41]. After the segmentation, each pixel is assigned to a region as shown in Fig. 4c. *Contour finding:* After the segmentation step, the contour between each segment is described by coordinates that quantify distinctive lines. Therefore, a contour-finding algorithm based on the two-dimensional Marching-Squares algorithm is applied [42]. Here, the image is divided into a uniform grid, where each pixel is located at the intersections of the resulting grid. The algorithm moves through this grid and decides how the contour line crosses each square of the grid based on four possible configurations. As a result, the segmented regions of the Random Walker are separated by distinctive lines (see Fig. 4d).

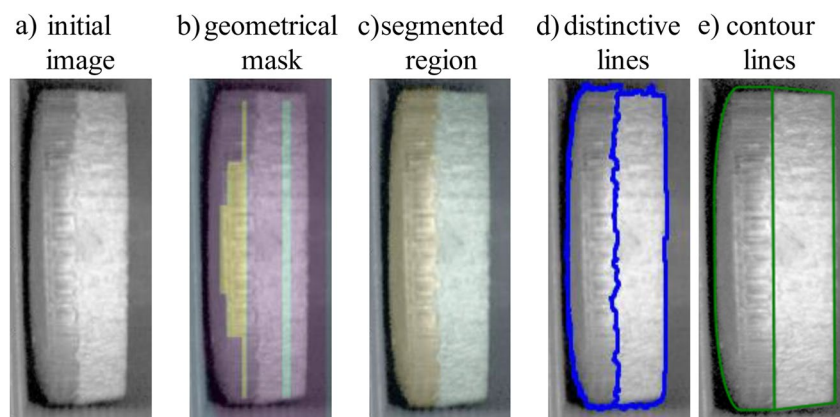
Parameterization: In the final step, the level-set method is used to parameterize the distinctive lines and to find a function that describes the shape of the segmented regions in the orthogonal and angular views. The level-set function describes the contour of a vertical section at the height z in a two-dimensional space, so that the final contour of the segmented region is described by the isoline $z = 0$. In this study, the level-set function $f(p_x, p_y)$ describes the contour of the segmented workpiece image as a function of the pixel position $p_x \in \{0, \dots, N_x - 1\}$ and $p_y \in \{0, \dots, N_y - 1\}$. Once the distinctive lines are interpolated and uniquely described by $f(p_x, p_y)$, the KPPs can be extracted from the image. Since the level-set function is defined by the two variables p_x and p_y , a conversion from pixels to millimeters is required. Preliminary tests for this work have shown that the diameter of the blanked part remains constant at a value of $6288 \pm 4.81 \mu\text{m}$ regardless of the prevailing wear state, so a constant conversion factor of $14.15 \mu\text{m}/\text{pixel}$ was used.

As a result of the transformation process, seven KPPs for the orthogonal view and nine KPPs for the angular view are available in absolute lengths in millimeters. Figure 5

Table 2 Identification and elimination of misplaced images

| Wear state | Total images | Kept images |
|------------------------|--------------|-------------|
| $r_1 = 0.0 \text{ mm}$ | 4061 | 1014 |
| $r_2 = 0.1 \text{ mm}$ | 3464 | 1556 |
| $r_3 = 0.2 \text{ mm}$ | 3360 | 1374 |
| $r_4 = 0.3 \text{ mm}$ | 4079 | 1570 |
| $r_5 = 0.4 \text{ mm}$ | 3873 | 1676 |
| $r_6 = 0.5 \text{ mm}$ | 3463 | 1311 |
| $r_7 = 0.6 \text{ mm}$ | 4172 | 713 |

Fig. 4 Random Walker algorithm combined with Marching-Squares algorithm for contour finding on a blanked surface (a) by defining a geometric mask (b) followed by segmentation of regions (c), determination of distinctive lines (d), and parameterization of the contour line (e)



summarizes the KPPs for both views. In the angular view, the KPPs are described by the height of the shear zone h_s^{ANG} , height of the shear fracture zone and burr $h_{f,b}^{\text{ANG}}$, diameter of the workpiece d^{ANG} , offset of the ellipse determines fracture zone and burr $s_{f,b}^{\text{ANG}}$, offset of the ellipse determines shear zone s_s^{ANG} , small axis of the ellipse determines shear zone e_s^{ANG} , small axis of the ellipse determines fracture zone e_f^{ANG} , small axis of the ellipse determines the burr e_b^{ANG} , and big axis of the ellipse determines the burr E_b^{ANG} . In the orthogonal view, the KPPs are described by the height of the rollover zone h_e^{ORTH} , height of the shear zone h_s^{ORTH} , the sum of the height of fracture zone and burr $h_{b,f}^{\text{ORTH}}$, total height of the workpiece h^{ORTH} , height of the width of the rollover zone w_e^{ORTH} , diameter of the workpiece d^{ORTH} , and the fracture angle α .

To ensure real-time extraction of KPP at high stroke rates, the computational effort for preprocessing and transformation must be estimated. Table 3 summarizes the absolute computation time. With the used computer resources (type, Intel Core i7 4770; used cores, 4; internal clock, 3.9 GHz; physical RAM, 16 GB; and average load, 80%), it takes 0.536 s to analyze a single pair of workpiece images and extract the 16 KPPs from both views. Assuming a stroke rate of 300 spm and a measurement interval of 120° , in which images must be captured and stored, this results in an absolute time of 0.15 s per stroke for preprocessing and transformation, which enables QA of every 4th part. To further increase the real-time capability of the system, the absolute time required to extract the KPPs from the blanked surface images can be drastically reduced by increasing the computer resources or using FPGA-based frame grabber.

Table 3 Computational effort for extracting KPP from image acquired with the proposed optical system

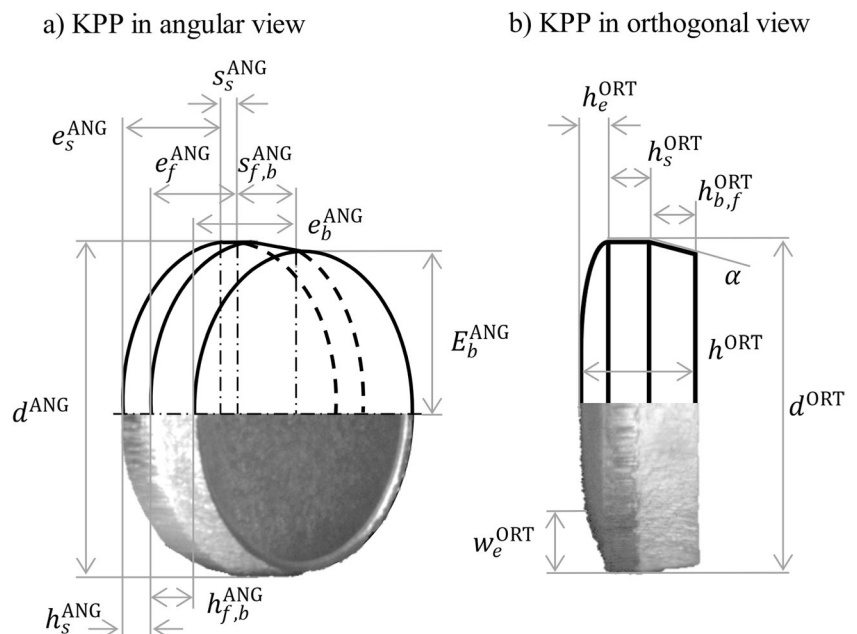
| Action | Computational time (s) |
|-----------------|------------------------|
| Preprocessing | 0.005 |
| Segmentation | 0.474 |
| Contour finding | 0.008 |
| Parametrization | 0.049 |
| Total time | 0.536 |

4 Suitability of KPP to quantify the quality of a blanked surface

To validate the accuracy of the optical system combined with the presented method, the extracted KPPs from the orthogonal view are compared with the same features obtained from microscope images. For microscopic measurement, microsections of the workpieces are made. The measurement is then performed by a confocal white microscope μsurf (nanofocus), which serves as the ground truth. According to the DIN EN 10140 (see Fig. 1), the rollover zone h_e^{ORTH} , the height of shear zone h_s^{ORTH} , the height of fracture zone h_f^{ORTH} , and height of the burr h_b^{ORTH} are used to quantify the quality of a blanked surface. The burr height is calculated from the difference between the initial height of the workpiece (2 mm), which is assumed to be constant, and the total height h^{ORTH} .

Figure 6 shows the four directly extracted features from the orthogonal views determined by the confocal microscope, colored in black, and the four KPPs extracted from

Fig. 5 KPP extracted from the workpiece images in angular (a) and orthogonal (b) view



the blackened surfaces with the developed system, colored in red. For the heights of the shear zone and the fracture zone, the average deviation from the ground truth is $\Delta h_s^{ORTH} = 8.59 \mu\text{m}$ for the shear zone and $\Delta h_f^{ORTH} = 25.28 \mu\text{m}$ for the fracture zone. Due to the rough boundary between these two zones, the Random Walker algorithm detects a parting line, but it varies greatly around the perimeter of the blanked workpiece. In addition to this fluctuating transition between the shear and fracture zones, an asymmetric clearance influences the shape of the parting line. Such asymmetric clearance is related to poor alignment of the punch to the die or adhesions on the lateral surface of the tool. For comparison, Fig. 7a shows the parting line for the wear state $r_2 = 0.1 \text{ mm}$ for a blanked workpiece with symmetrical (left) and asymmetrical (right) circumferences. In this case, the variation in the parting line is caused by temporary adhesions on the lateral surface of the blanking tool. As a result of the narrowed clearance at the point of adhesion, compressive and tensile stresses are superimposed, causing the material to flow longer, and creating a locally pronounced shear zone. For the rollover zone, an average deviation from the ground truth of $\Delta h_e^{ORTH} = 13.63 \mu\text{m}$ is achieved. Due to the low contrast between the shear zone and the rollover zone, the boundary between these two zones is difficult for the algorithm to recognize, resulting in an increased variation. Figure 7b shows this phenomenon, which is mainly caused

by the lighting scene and thus related to the illumination design of the optical system.

In the literature, burr height is defined as a critical parameter for the customer. Excessive increase in burr height results in handling with risk of injury and inability to achieve functional and geometric target requirements. During the tests, an average deviation from the ground truth of $\Delta h_b^{ORTH} = 26.74 \mu\text{m}$ is obtained. The deviation is caused by a jagged edge of the burr and hinders the detection of a sharp end contour. This effect is particularly pronounced as the wear on the tool cutting edge increases. Figure 7c shows the formation of the end contour of the burr for the wear states $r_2 = 0.1 \text{ mm}$ and $r_6 = 0.5 \text{ mm}$. Up to a wear state of $r_6 = 0.50 \text{ mm}$, the average deviation from the ground truth is only $20.44 \mu\text{m}$ or 1% of the original sheet thickness. In practice, a value of 10% burr, relative to the initial sheet thickness, is often declared critical, so that with the results obtained, a burr is detected well before the rejection criterion occurs. As already explained in the objective of this work, the quantification of the KPPs of the cutting surface is not limited to the base area of the workpiece (dimension of the workpiece in the x-y plane), but only to the thickness of the initial semi-finished product. In the case of the optical system proposed in this study, a value of $\pm 20.44 \mu\text{m}$ is obtained with a probability of 96%, by which the measured burr height varies. This means that with a maximum tolerable burr height of 10% of the sheet thickness, the minimum

Fig. 6 Comparison between the KPPs of the blanked surface extracted with the optical system combined with the presented method (red line) and directly extracted with the confocal microscope μSurf (black line)

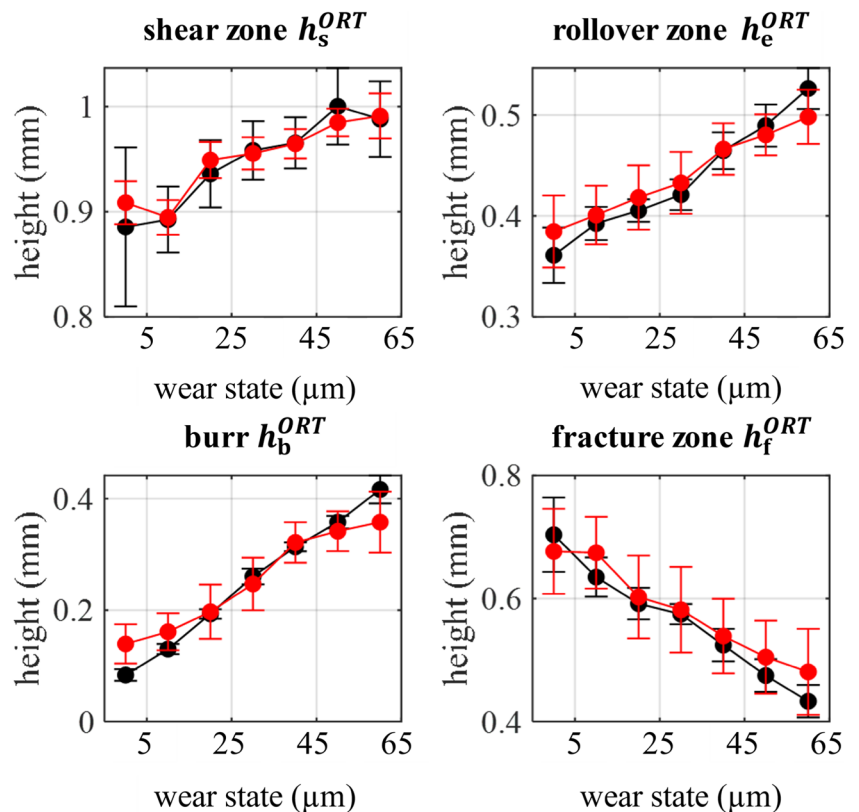
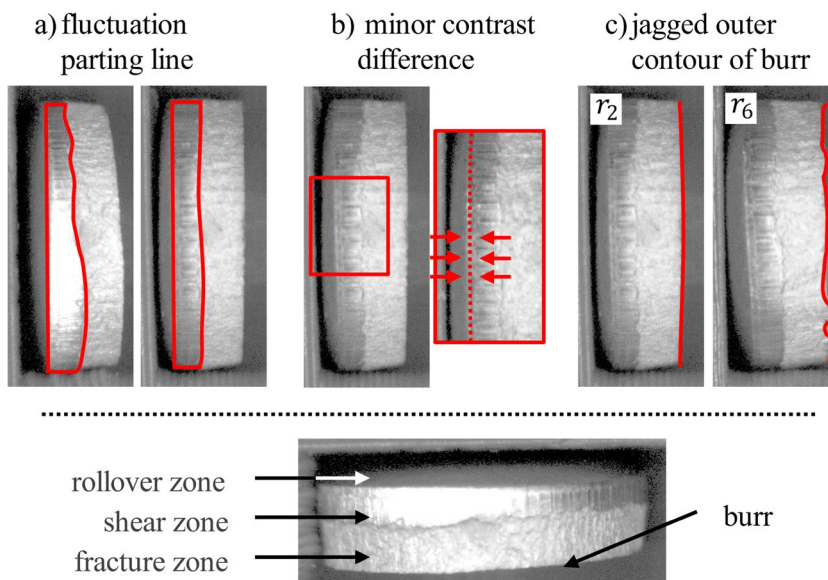


Fig. 7 Effects that lead to the deviation between the KPP directly derived from the work-piece images and determined by the reflected light microscope (reference)



sheet thickness of the blanked components to be monitored must be greater than 0.25 mm.

At this stage, it should already be pointed out that the definition of standard limits for each wear state at which a quantification of the blanked surface by the optical system is still considered trustworthy must be carried out for the individual KPP on a company-specific and product-dependent basis. Since the optical system is only designed to describe the characteristics of the blanked surface, fluctuations in the KPPs can be detected and quantified, but the cause of such a fluctuation cannot be distinguished.

5 Wear state detection using ML models

As shown in Section 4, the KPPs extracted from the blanked surface can be used to directly describe the quality of the workpiece and thus for QA. Since there is a relationship between the KPPs and the current wear state, as shown in Fig. 1 and Fig. 6, the KPPs are used to estimate the rounding at the cutting edge. As the wear state depends on many parameters and there is a non-linear function between the input variable cutting edge radii r and the KPPs of the blanked surface, ML models are used for the estimation. At this point, reference should be made to previous work where the development procedure for ML models for cutting radii estimation is discussed in detail [43]. Since the use of ML models in this paper is only used as a validation method for the quality of the extracted KPPs, the authors refer to these studies for further information. To find the most appropriate model for this use case, a two-step model optimization is performed. In the first step, nine models, including a random forest (RF), linear discriminant analysis (LDA), naive Bayes (NB), linear SVM (lSVM), quadratic SVM (qSVM), cubic

SVM (cSVM), k-nearest neighbor (KNN), a one-layer neural network (1NN), and a three-layer neural network (3NN), are trained based on their default parameter configuration. The reference configuration of the selected ML models in the Python library Scikit-Learn can be found in Table 4.

In a second step, the best fitting model is optimized by hyperparameter optimization. All models are trained on a labeled data set, where the input is defined by the 16 KPPs (see Fig. 5) and the wear state is quantified by the cutting edge radii. Figure 8 demonstrates the accuracy achieved by a fivefold cross-validation, where the wear state is best estimated by a qSVM with $91.82 \pm 0.11\%$. By further hyperparameter optimization, the classification accuracy for the optimized qSVM (qSVM-opt) is increased to $92.79\% \pm 0.14\%$.

If we take a closer look at the performance of qSVM-opt using the confusion matrix of the classification shown in Fig. 9, we can see that the error is mainly due to the misclassification of neighboring wear states, and an accumulation of misclassifications is found along the diagonal of the matrix. Thus, misclassified states are only one class away from the target class. Especially for small cutting radii, the classification task is challenging. For low wear states, the differences between the KPPs are small. In particular, the formation of a burr, which is clearly visible with increasing cutting edge radii, is an important way of describing the wear state. This trend can also be seen in the comparison between the KPPs and the ground truth in Fig. 6.

6 Conclusions and outlook

Since the inline extraction of quality parameters blanking, represented by features of the blanked surface, is not yet used in practice due to four requirements: *installation*

Table 4 Reference configuration of the selected ML models based on the Scikit-Learn environment during the first step of model optimization

| ML model | |
|------------------------------|---|
| Random forest | n_estimators=100, criterion='gini' |
| Linear discriminant analysis | solver='svd' |
| Naive Bayes | var_smoothing=1e-09 |
| Linear SVM | C=1.0, kernel='linear', degree=3, gamma='scale', coef0=0.0, shrinking=True, tol=0.001, decision_function_shape='ovr' |
| Quadratic SVM | C=1.0, kernel='poly', degree=2, gamma='scale', coef0=0.0, shrinking=True, tol=0.001, decision_function_shape='ovr' |
| Cubic SVM | C=1.0, kernel='poly', degree=3, gamma='scale', coef0=0.0, shrinking=True, tol=0.001, decision_function_shape='ovr' |
| k-nearest neighbor | n_neighbors=5, weights='uniform', algorithm='auto', leaf_size=30, p=2, metric='minkowski' |
| One-layer neural network | hidden_layer_sizes=(100,), activation='relu', solver='adam', alpha=0.0001, batch_size='auto', learning_rate='constant', learning_rate_init=0.001, power_t=0.5, tol=1e-4 |
| Three-layer neural network | hidden_layer_sizes=(100,), activation='relu', solver='adam', alpha=0.0001, batch_size='auto', learning_rate='constant', learning_rate_init=0.001, power_t=0.5, tol=1e-4 |

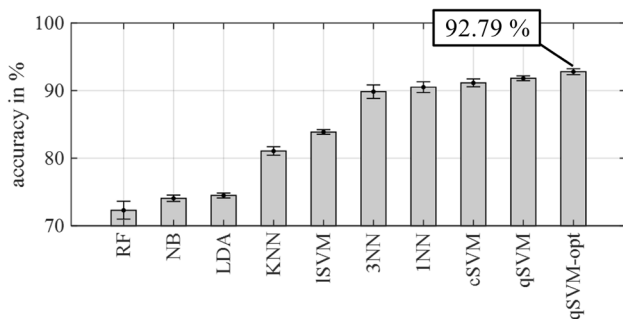


Fig. 8 Classification results obtained for each tested ML model

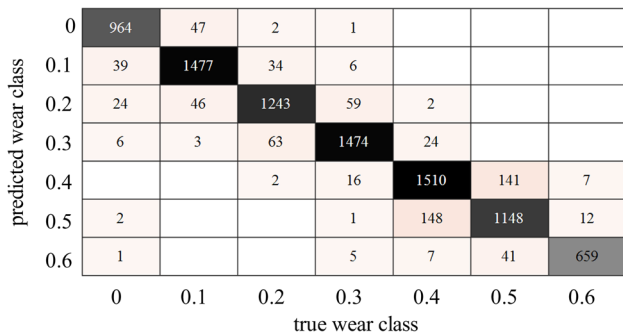


Fig. 9 Cumulative confusion matrix for wear state classification of qSVM-opt quantifying the number of misclassifications

space, blanking surface, system dynamics, and cost, this work proposes an optical system in combination with a novel analysis methodology to fill this gap. The system allows real-time quality assurance of blanked parts up to 300 spm, although in this work the analysis is limited to every 4th workpiece due to the available computing resources. During the development of the optical system,

the authors took care to use commercially available, low-cost components and to keep the total cost of the system below \$800. For the analysis of the acquired image data, the applied methodology consists of the steps of preprocessing and transformation, where the transformation is divided into the steps of *segmentation*, *contour finding* and *parameterization*. The quality of the KPPs extracted by this method is validated by two use cases. In the first case, the extracted KPPs are compared with a ground truth obtained by a confocal microscope. Here, deviations from the ground truth of $\Delta h_e^{ORTH} = 13.63 \mu\text{m}$ from the height of the rollover zone, $\Delta h_s^{ORTH} = 8.59 \mu\text{m}$ from the height of the shear zone, $\Delta h_f^{ORTH} = 25.28 \mu\text{m}$ from the height of the fracture zone, and $\Delta h_b^{ORTH} = 26.74 \mu\text{m}$ from the height were achieved. In the second case, several ML models were built based on the extracted KPPs to classify the wear state of the blanking tool. Using an optimized SVM (qSVM-opt), the seven cutting edge radii were assigned to the correct wear state on the tool with an accuracy of 92.80%. In addition to this accurate estimation, the model accumulated almost all observations around the diagonal of the confusion matrix. Thus 92.80% are found on the main diagonal (correctly classified), 7.11% are directly above or below the main diagonal (one class next to the target class), and only 0.09% are further away from the diagonal.

To also obtain a conclusion about the cause of a fluctuation in the KPP in the future and to relate the characteristics of the blanked surface to the current process state, it is necessary to vary targeted parameters such as stroke speed, clearance, cutting line geometry, or semi-finished product properties. By using advanced segmentation methods, a detailed description of the cutting surface is possible, so that the system will not only be able to quantify the properties of the cutting surface, but also to describe its origin.

Acknowledgements The results of this paper were achieved within the project “Mittelstand 4.0-Kompetenzzentrum Darmstadt” funded by the German Federal Ministry of Economic Affairs and Climate Action (BMWK) and within the project “Stamping Insights” funded by the German Federal Ministry of Education and Research (BMBF). In addition, the authors would like to thank Bruderer AG for providing the BSTA 810-145 high-speed press, Dayton Progress GmbH for providing the parts for the blanking tool components, and Kistler AG for providing the measuring equipment to record data sets even under difficult conditions.

Author contributions All authors contributed equally to the concept and design of the study, and to the data collection and analysis. The first draft of the manuscript was written by CK. All authors read and approved the final manuscript.

Funding Open Access funding enabled and organized by Projekt DEAL. The research leading to these results was funded by the German Federal Ministry of Economic Affairs and Climate Action (project “Mittelstand Kompetenzzentrum 4.0 Darmstadt” under grant no. 01MF15005A) and the German Federal Ministry of Education and Research (project “Stamping Insights” under grant no. 13N16563).

Declarations

Competing interests The authors declare no competing interests.

Open Access This article is licensed under a Creative Commons Attribution 4.0 International License, which permits use, sharing, adaptation, distribution and reproduction in any medium or format, as long as you give appropriate credit to the original author(s) and the source, provide a link to the Creative Commons licence, and indicate if changes were made. The images or other third party material in this article are included in the article’s Creative Commons licence, unless indicated otherwise in a credit line to the material. If material is not included in the article’s Creative Commons licence and your intended use is not permitted by statutory regulation or exceeds the permitted use, you will need to obtain permission directly from the copyright holder. To view a copy of this licence, visit <http://creativecommons.org/licenses/by/4.0/>.

References

- Altan T, Tekkaya AE (2012) Sheet metal forming. ASM International, Ohio
- Groche P, Hohmann J, Recklin V, Schmidt W, Brenneis M, Traub T, Kramer P (2016) Spatially resolved force sensing in forming processes. In: Liewald M (ed) Proceedings of the 49th plenary meeting of the international cold forging group. Institute for Metal Forming Technology, Stuttgart, pp 178–183
- Stahl J, Pätzold I, van den Bosch L, Kindsmüller A, Golle R, Volk W (2021) The frictional force between slug and die in shear cutting after material separation. *KEM* 883:285–293. <https://doi.org/10.4028/www.scientific.net/KEM.883.285>
- Kubik C, Molitor DA, Rojahn M, Groche P (2022) Towards a real-time tool state detection in sheet metal forming processes validated by wear classification during blanking. *IOP Conf Ser Mater Sci Eng* 1238:12067. <https://doi.org/10.1088/1757-899X/1238/1/012067>
- Faura F, López J, Sanes J (1997) Criterion for tool wear limitation on blanking 18-8 stainless steel strips. *Rev Metal* 33:304–310. <https://doi.org/10.3989/revmetalm.1997.v33.i5.842>
- Jemielniak K (1999) Commercial tool condition monitoring systems. *Int J Adv Manuf Technol* 15:711–721. <https://doi.org/10.1007/s001700050123>
- Panda A, Olejárová Š, Valíček J, Harničárová M (2018) Monitoring of the condition of turning machine bearing housing through vibrations. *Int J Adv Manuf Technol* 97:401–411. <https://doi.org/10.1007/s00170-018-1871-7>
- Lee WB, Cheung CF, Chiu WM, Chan LK (1997) Automatic supervision of blanking tool wear using pattern recognition analysis. *Int J Mach Tool Manuf* 37:1079–1095. [https://doi.org/10.1016/S0890-6955\(97\)88104-7](https://doi.org/10.1016/S0890-6955(97)88104-7)
- Groche P, Hohmann J, Übelacker D (2019) Overview and comparison of different sensor positions and measuring methods for the process force measurement in stamping operations. *Measurement* 135:122–130. <https://doi.org/10.1016/j.measurement.2018.11.058>
- Demmel P, Hirsch M, Golle R, Hoffmann H (2012) In situ temperature measurement in the shearing zone during sheet metal blanking. *AMR* 445:207–212. <https://doi.org/10.4028/www.scientific.net/AMR.445.207>
- Sari DY, Wu T-L, Lin B-T (2017) Preliminary study for online monitoring during the punching process The International. *Int J Adv Manuf Technol* 88:2275–2285. <https://doi.org/10.1007/s00170-016-8956-y>
- Wuest T, Weimer D, Irgens C, Thoben K-D (2016) Machine learning in manufacturing: advantages, challenges, and applications. *Prod Manuf Res* 4:23–45. <https://doi.org/10.1080/21693277.2016.1192517>
- Koh CKH, Shi J, Black J (1996) Tonnage signature attribute analysis for stamping process. *Transaction of North American Manufacturing Research Institution of SME* 24:193–198
- Ge M, Du R, Zhang G, Xu Y (2002) Fault diagnosis using support vector machine with an application in sheet metal stamping operations. *MSSP* 18:143–159. [https://doi.org/10.1016/S0888-3270\(03\)00071-2](https://doi.org/10.1016/S0888-3270(03)00071-2)
- Hambli R (2002) Prediction of burr height formation in blanking processes using neural network. *Int J Mech Sci* 44:2089–2102. [https://doi.org/10.1016/S0020-7403\(02\)00168-6](https://doi.org/10.1016/S0020-7403(02)00168-6)
- Kubik C, Knauer SM, Groche P (2021) Smart sheet metal forming: importance of data acquisition, preprocessing and transformation on the performance of a multiclass support vector machine for predicting wear states during blanking. *J Intell Manuf.* 33:259–282. <https://doi.org/10.1007/s10845-021-01789-w>
- Huang C-Y, Dzulfikri Z (2021) Stamping monitoring by using an adaptive 1D convolutional neural network. *Sensors* 21:262. <https://doi.org/10.3390/s21010262>
- Niemietz P, Unterberg M, Trauth D, Bergs T (2021) Autoencoder based wear assessment in sheet metal forming. *IOP Conf Ser Mater Sci Eng* 1157:12082. <https://doi.org/10.1088/1757-899X/1157/1/012082>
- Catalucci S, Thompson A, Piano S, Branson DT, Leach R (2022) Optical metrology for digital manufacturing: a review. *Int J Adv Manuf Technol* 120:4271–4290. <https://doi.org/10.1007/s00170-022-09084-5>
- Tran T-T, Ha C (2018) Non-contact gap and flush measurement using monocular structured multi-line light vision for vehicle assembly. *Int J Control Autom Syst* 16:2432–2445. <https://doi.org/10.1007/s12555-017-0535-y>
- Mannan MA, Kassim AA, Jing M (2000) Application of image and sound analysis techniques to monitor the condition of cutting tools. *Pattern Recognit Lett* 21:969–979. [https://doi.org/10.1016/S0167-8655\(00\)00050-7](https://doi.org/10.1016/S0167-8655(00)00050-7)
- Chen JY, Chang WY, Lee BY, Lin CS (2012) Optical image inspection of cutting tool geometry for grinding machines. *AMR* 579:235–242. <https://doi.org/10.4028/www.scientific.net/AMR.579.235>

23. Gupta M, Raman S (2001) Machine vision assisted characterization of machined surfaces. *Int J Prod Res* 39:759–784. <https://doi.org/10.1080/00207540010011045>
24. Lee SG, Mao Y, Gokhale AM, Harris J, Horstemeyer MF (2009) Application of digital image processing for automatic detection and characterization of cracked constituent particles/inclusions in wrought aluminum alloys. *Mater Charact* 60:964–970. <https://doi.org/10.1016/j.matchar.2009.03.014>
25. Myant C, Fowell M, Spikes HA, Stokes JR (2010) An investigation of lubricant film thickness in sliding compliant contacts. *Tribol Trans* 53:684–694. <https://doi.org/10.1080/10402001003693109>
26. Mohan A, Poobal S (2018) Crack detection using image processing: a critical review and analysis. *Alex Eng J* 57:787–798. <https://doi.org/10.1016/j.aej.2017.01.020>
27. Qiu T, Lai X, Ni J (2020) Machine learning based novelty detection methods for progressive stamping process. *MSEC2020-8496*. 84263:V002T07A034. <https://doi.org/10.1115/MSEC2020-8496>
28. Molitor DA, Kubik C, Hetfleisch RH, Groche P (2022) Workpiece image-based tool wear classification in blanking processes using deep convolutional neural networks. *Prod Eng Res Devel* 88:2275. <https://doi.org/10.1007/s11740-022-01113-2>
29. Lorenz M, Menzl M, Donhauser C, Layh M, Pinzer BR (2022) Optical inline monitoring of the burnish surface in the punching process. *Int J Adv Manuf Technol* 118:3585–3600. <https://doi.org/10.1007/s00170-021-07922-6>
30. Kubik C, Molitor DA, Becker M, Groche P (2022) Knowledge discovery from time series in engineering applications using machine learning techniques. *J Manuf Sci Eng* 144:091003. <https://doi.org/10.1115/1.4054158>
31. Weiss HA, Leuning N, Steentjes S, Hameyer K, Andorfer T, Jenner S, Volk W (2017) Influence of shear cutting parameters on the electromagnetic properties of non-oriented electrical steel sheets. *J Magn Magn Mater* 421:250–259. <https://doi.org/10.1016/j.jmmm.2016.08.002>
32. Hohmann J, Schatz T, Groche P (2017) Intelligent wear identification based on sensory inline information for a stamping. *NEWTECH 2017*. https://doi.org/10.1007/978-3-319-56430-2_21
33. German Institute for Standardization DIN EN 10140 (2006) Cold rolled narrow steel strip - tolerances on dimensions and shape. Beuth Verlag. <https://www.beuth.de/de/norm/din-iso-11040-4/272400677>. Accessed 08 Nov 2023
34. Hambli R (2002) Design of experiment based analysis for sheet metal blanking processes optimisation. *Int J Adv Manuf Syst* 19:403–410. <https://doi.org/10.1007/s001700200041>
35. Mucha J (2010) An experimental analysis of effects of various material tool's wear on burr during generator sheets blanking. *Int J Adv Manuf Technol* 50:495–507. <https://doi.org/10.1007/s00170-010-2554-1>
36. Hernández JJ, Franco P, Estrems M, Faura F (2006) Modelling and experimental analysis of the effects of tool wear on form errors in stainless steel blanking. *J Mater Process Technol* 180:143–150. <https://doi.org/10.1016/j.jmatprotec.2006.05.015>
37. Kubik C, Hohmann J, Groche P (2021) Exploitation of force displacement curves in blanking—feature engineering beyond defect detection. *Int J Adv Manuf Syst* 113:261–278. <https://doi.org/10.1007/s00170-020-06450-z>
38. Feistle M, Koslow I, Krinninger M, Golle R, Volk W (2017) Reduction of burr formation for conventional shear cutting of boron-alloyed sheets through focused heat treatment. *Proc CIRP* 63:493–498. <https://doi.org/10.1016/j.procir.2017.03.161>
39. Klingenberg W, de Boer TW (2008) Condition-based maintenance in punching/blanking of sheet metal. *Int J Mach Tools Manuf* 48:589–598. <https://doi.org/10.1016/j.ijmactools.2007.08.013>
40. Yoo J-C, Han TH (2009) Fast normalized cross-correlation. *CSSP* 28:819–843. <https://doi.org/10.1007/s00034-009-9130-7>
41. Wechsler H, Kidode M (1979) A random walk procedure for texture discrimination. *IEEE Trans Pattern Anal Mach Intell* 1:272–280. <https://doi.org/10.1109/TPAMI.1979.4766923>
42. Maple C (2003) Geometric design and space planning using the marching squares and marching cube algorithms. 2003 International Conference on Geometric Modeling and Graphics. Proceedings, London, pp 90–95. <https://doi.org/10.1109/GMAG.2003.1219671>
43. Kubik C, Becker M, Molitor D-A, Groche P (2022) Towards a systematic approach for wear detection in sheet metal forming using machine learning. *Prod Eng Res Devel* 4:337. <https://doi.org/10.1007/s11740-022-01150-x>

Publisher's Note Springer Nature remains neutral with regard to jurisdictional claims in published maps and institutional affiliations.